Journal of the European Ceramic Society 21 (2001) 251–261

www.elsevier.com/locate/jeurceramsoc

Impact response and mechanical behavior of 3-D ceramic matrix composites

Hsien-Kuang Liu *, Chuan-Cheng Huang

Department of Mechanical Engineering, Feng-Chia University, 100 Wenhwa Road, 407 Taichung, Taiwan

Received 29 September 1999; received in revised form 24 May 2000; accepted 4 June 2000

Abstract

This paper examines the impact response, compressive strength, and flexural strength of three-dimensional carbon fiber reinforced ceramics. The composite was fabricated by combination of the pressure infiltration method and sol–gel processing, using the mixture of silica sol and alumina particles. The effects of sol viscosity on impact response and flexural strength, and infiltration pressure on compressive strength are investigated. Impact tests were carried out using an Izod impact testing machine. It is found that impact energy of the specimens increases linearly with sol viscosity. The sol viscosity affects impact response by two factors, interfacial strength and volume fraction of silica. Higher sol viscosity leads to weaker interface and more residual silica, resulting in higher impact energy. Flexural strength decreases with sol viscosity according to an exponential decay function because higher viscosity leads to weak interface as well as lower flexural strength. Compressive strength increases with infiltration pressure, which follows a parabolic function. Higher infiltration pressure enhances infiltration of the mixture, resulting in dense matrix and strong interface. As a result, the composite shows a higher compressive strength due to less buckling of longitudinal fibers strongly confined by neighboring dense matrix and transverse fiber bundles. The compressive stress-strain history has been examined and related to how the specimens respond to the compression.

Keywords: Alumino-silicate matrix; Carbon fibre; Composites; Mechanical properties; Sol–gel methods

1. Introduction

To fabricate ceramic matrix composites by combination of pressure infiltration method and sol–gel processing takes advantages of both methods.[1–3] The advantages include variety of reinforcement, low densification temperature, low shrinkage, and reduced drying stresses. Authors have fabricated three-dimensional (3-D) green ceramic matrix composites[1] and short fiber ceramic matrix composites[2] by combination of both methods, using the mixture of sol and ceramic particles. In the former study, interparticle forces and particle size distribution are the major factors that influence green density and drying stresses; while in the latter study, sedimentation, infiltration rate, and viscosity of mixture of sol and ceramic particles are the major factors that influence mechanical properties of composites. Furthermore, the mixture of sol and ceramic particles was found to have different behavior during the consolidation process[3] compared to that of a slurry.[4] The latter demonstrated that the slurry during consolidation must have a sufficiently high viscosity to prevent sedimentation and lower packing density. However, in our studies for the short fiber composite it was proved that high viscosity of the mixture of sol and ceramic particles leads to the reaction of sol with ceramic particles, and therefore more sedimentation and low packing density. Therefore, one of the goals of this work is to study the influence of sol viscosity on microstructure and mechanical properties of 3-D ceramic matrix composites.

Recently, major progress has been made in the development of 3-D ceramic matrix composites. The driving forces behind the development of these materials have been the need for high strength and high energy absorption under multidirectional loadings, and conformity for shape forming.[5] The preform used in the composite creates 3-D networks of reinforcing fibers that eliminate weak planes and prevent the material from planar type of failure, such as delamination. In the absence of weak planes, the impact energy could be dissipated in a more localized area.[6] Whether or not a 3-D ceramic matrix

* Corresponding author.
E-mail address: hkliu@fcu.edu.tw (H.-K. Liu).

0955-2219/01/$ - see front matter
PII: S0955-2219(00)00181-3

composite is more impact resistant depends not only on the constituents used but, more important, on how the network is constructed and how the impact load is applied. It is therefore the goal of this research to characterize the impact behavior of the materials.

A review of literature indicates that most previous research was dedicated to the impact behavior of unidirectional or 2-D ceramic composites,[7–9] but very little has been done on that of 3-D ceramic composites. The major reason is the difficulty in preparing specimens suitable for impact tests. For 3-D ceramic composites under Charpy impact testing,[9] several interesting conclusions were proposed. First, the matrix is divided by the 3-D network structure and increases dynamic toughness of the composite. Second, the compliant fiber network raises the resistance to crack propagation. Third, the coating of fiber improves impact resistance. Fourth, fiber pull-out increases impact resistance. Damaged by delamination, 2-D C/C composite has higher impact rupture work than that of 3-D C/C composite. For cross-ply ceramic composites under drop-weight impact,[7] high temperature environment and applied tensile loading make the damage of the composite more severe. This indicates that different testing conditions significantly influence the impact response of the materials.

To deeply understand impact response of the materials, static tests are necessary. For ceramic matrix composites under compression,[10] dilatational fracture within the matrix dominates composite failure at low confinement pressures, while fiber kinking caused by high confinement pressure indicates shear dominated mechanisms. The processing and mechanical properties of 3-D carbon/SiC and carbon/Si_3N_4 at high temperature under vacuum[11] and fracture processes of cross-weave carbon/SiC were reviewed.[12] Flexural strengths of 3-D carbon/SiC at room and high temperatures are much lower than those unidirectional carbon/SiC composites. The high-temperature strength is higher than that at room temperature for 3-D carbon/SiC, while the trend is reverse for 3-D carbon/Si3N4. The fracture process of cross-weave carbon/SiC does not involve cracking by a single dominant crack but occurs by the development of multiple transverse fractures of groups of four to eight fibers followed by longitudinal cracking at the interface. The cracks were temporary arrested by the internal voids until specimens fail and there is extensive fiber debonding and pull-out. Although ceramic matrix composites reinforced by carbon fibers are vulnerable to degradation in an oxidizing environment at relatively low temperatures, they provide valuable information for the material used in oxygen free environment as well as for other material systems.

Based on the knowledge we have gained, the prime objective of this work is aimed at evaluating impact response, flexural strength, and compressive strength of 3-D woven ceramic matrix composites fabricated by pressure infiltration and sol–gel methods. The effect of sol viscosity and infiltration pressure on mechanical properties of composites is studied. The correlation between mechanical properties and damage modes of composites is investigated.

2. Experimental procedure

2.1. Materials

The silica sol was prepared by the following recipe in which tetraethyl-orthosilicate (TEOS), ethanol, deionized water and 7 wt.% of HNO_3 were mixed and stirred at a volume ratio of 1:1:1.6:0.06 to obtain 175 ml sol. In order to study the effect of sol viscosity on mechanical properties of 3-D ceramic matrix composites, four kinds of viscosity are selected. The sol with viscosity 3.78 cP was obtained according to the procedure above, while sols with viscosities 4.17 and 8.5 cP are prepared by evaporating 250 and 350 ml sols, respectively, to 175 ml. The lowest viscosity 3.02 cP was prepared by changing volume ratio of TEOS from 1.0 to 0.25. 17 g of alumina particles (α-Al_2O_3, average diameter $d = 0.3$ μm, purity = 99.99%, $\rho = 3.965$ g/cm^3, ProChem Co., USA) were added to the sol to prepare the infiltrate. The infiltrate was further mixed both in an ultrasonic bath and electromagnetic blender in turns until the particles in the infiltrate were dispersed uniformly and well wetted. The carbon fiber used in the 3-D preform is Toho T-300 fiber. The properties of fiber are as follows: tensile strength 3920 MPa, tensile modulus 235 GPa, diameter (d) = 7 μm, $\rho = 1.77$ g/cm^3, 12000 filaments in a fiber tow. The 3-D preform is a three-axis orthogonal structure. Fiber volume fraction of the 3-D preform is 38.2%. A one-shuttle weaving scheme is adopted to fabricate the 3-D fabric.[6]

In order to predict volume fraction of silica in the silica/alumina matrix, solid content in the silica sol was measured. A drying and sintering experiment was conducted on the silica sol with four kinds of viscosity. The silica sol was dried at 80°C to obtain dried gel. Thereafter the dried gel was sintered at 1300°C for 2 h to yield silica. The volume of silica sol was controlled as 175 cm^3 (ml), and the weight of dried gel and silica were measured. Therefore volume of silica can be obtained with its density of 2.2 g/cm^3. These data are shown in Table 1.

2.2. Fabrication

A pressure infiltration apparatus was used to perform the processing of 3-D ceramic matrix composites. The apparatus consists of a cylinder with an inner diameter of 50 mm, a base cavity for collecting the liquid, a plunger, and a filter assembly. The filter assembly consists of nitrate cellulose membrane filter paper with pore

Table 1
Summary of mechanical properties of 3-D ceramic matrix composites

Specimen type	Sol viscosity (cP)[a]	Infiltration pressure	Green composite density (%)	Flexural strength (MPa)[b]	Flexural modulus (GPa)	Impact energy (J)	Impact energy/area (J/m^2)	Compression strain (%)	Compression strength (MPa)	Compression modulus (MPa)
BA	3.02	1.25 MPa	78.1	23.92	1.483					
BB	3.78	1.25 MPa	74.1	19.82	0.840					
BC	4.17	1.25 MPa	73.4	19.03	0.793					
BD	8.50	1.25 MPa	70.0	18.27	0.694					
IA	3.02	1.25 MPa	78.1			0.598	8813.81			
IB	3.78	1.25 MPa	74.1			0.721	9455.59			
IC	4.17	1.25 MPa	73.4			0.733	9502.57			
ID	8.50	1.25 MPa	70.0			0.775	10590.16			
PA	3.02	0.50 MPa[2]	71.9					3.51	24.97	1.392
PB	3.02	0.75 MPa	73.7					2.35	27.32	1.496
PC	3.02	1.00 MPa	76.8					2.43	31.07	3.042
PD	3.02	1.25 MPa	78.1					3.53	37.69	4.065

[a] cp, centi-Poise, unit of sol viscosity.
[b] MPa, Mega Pascal, unit of infiltration pressure.

size of 0.1 μm, a stainless steel wire cloth, and a perforated solid steel disk. The filter assembly was placed on the top of the base cavity. The stainless steel wire cloth was used to keep the filter paper from rupturing. Cylinder, filter assembly, and base were tightly sealed by thread and O-ring. The 3-D fabric was cut as a rectangle with dimension 3.8×2.5×0.85 cm, and then inserted into a rectangular hole within a circular acrylic disk with 5.0 cm in diameter and 0.85 cm thick. The fabric and disk were put in the cylinder and attached to the filter assembly closely. The infiltrate was then poured into the cylinder and an MTS testing machine set at constant pressure mode was used to provide the infiltration pressure on the plunger. Four kinds of infiltration pressure were used: 0.5, 0.75, 1.0 and 1.25 MPa. The infiltration procedure stops when the plunger reaches the upper surface of the fabric. Using pressure infiltration, the thick 3-D fabric can be efficiently infiltrated and consolidated via silica sol/alumina particle route in a single step. After infiltration, the green composite is dried in an oven at 60°C and humidity 95% for 24 h. In order to raise solid content, the dried composite is soaked into silica sol under vacuum for 3 h and then dried for 24 h.

Densification of the composite was conducted by a hot pressing furnace (FCPHP-R-5, FRET-20, High Multi 5000, Multi-purpose High Temperature Furnace, Japan). Conditions for hot pressing are temperature 1600°C and pressure 10 MPa for $1\frac{1}{2}$ h by flowing nitrogen gas. After hot pressing, mechanical properties and microstructure of composites were evaluated.

2.3. Characterization

2.3.1. Impact test

The impact tests were conducted using an Izod test machine (Model: TMI-43-01, Test Machine Co., USA). The dimension of specimens is 40 mm in length (L), 12 mm in width (b), and 7 mm in thickness (h). The specimens were clamped perpendicularly at one end, and left 30 mm free for the impact. The mass of the impactor, a pendulum, was 4.54 kg. After the pendulum impacted the specimen at top 10 mm, a pointer can read the impact energy on the machine based on the difference of the height of the pendulum before and after the impact. Four different specimens (IA, IB, IC, and ID) were impacted, which were fabricated by sol viscosity of 3.02, 3.78, 4.17, and 8.50 cP, respectively. First letter "I" in the specimen number means impact.

2.3.2. Compressive test

The dimension of specimens for compression is 37.5×24×7 mm ($L \times b \times h$). The compression loading is applied in the length direction, and both ends are gripped by the fixture for 15 mm in the through-thickness direction. The test is conducted by Instron 4468 testing machine and crosshead speed is set at 0.1 mm/s. Compressive strength σ and compressive modulus E are calculated by the following formula

$$\sigma = \frac{P}{bh} \tag{1}$$

$$E = \frac{P}{\delta}\frac{L}{bh} \tag{2}$$

where P is maximum load, P/δ is the slope on the compressive load–displacement curve at final stage. Four different specimens PA, PB, PC, and PD were compressed, which were fabricated by infiltration pressure of 0.50, 0.75, 1.0, and 1.25 MPa, respectively.

2.3.3. Flexural test

The dimension of specimens for three-point bending test is 40×12×7 mm ($L \times b \times h$). The span is 30 mm.

The test is conducted by Instron 4468 testing machine and crosshead speed is set at 0.008 mm/s. Flexural strength σ and flexural modulus E are calculated by the following formula

$$\sigma = \frac{3}{2}\frac{PL}{bh^2} \tag{3}$$

$$E = \frac{P}{\delta}\frac{L^3}{4bh^3} \tag{4}$$

where p is maximum load, P/δ is the initial slope on the load–displacement curve. Four different specimens BA, BB, BC, and BD were tested, which were fabricated by sol viscosity of 3.02, 3.78, 4.17, and 8.50 cP, respectively.

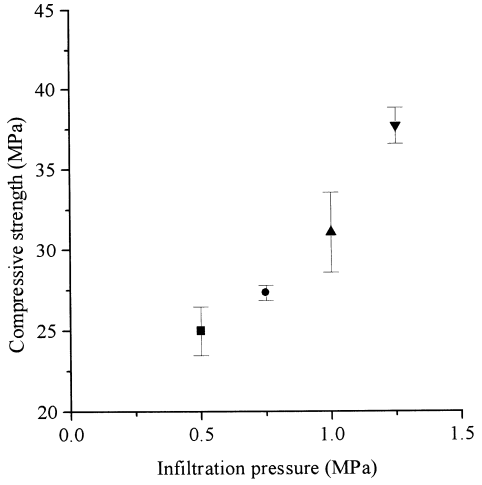

Fig. 1. Compressive strength as a function of infiltration pressure for 3-D ceramic matrix composites.

3. Results and discussion

Table 1 summarizes the effect of infiltration pressure on compressive strength, and sol viscosity on flexural strength and impact response of 3-D ceramic matrix composites (CMC). Green composite density of each specimen is also listed. The correlation among two processing parameters and three mechanical properties are discussed as follows.

3.1. Compressive strength and damage

As shown in Fig. 1, compressive strength of PA, PB, PC, and PD specimens increases with infiltration pressure according to a parabolic function. Compressive stress–strain curves for four specimens are shown in Fig. 2. In the curve for the PD specimen fabricated by the highest infiltration pressure of 1.25 MPa, the peak value and slope near the peak value lead to its highest compressive strength and modulus, respectively. Based on our observation, the damage of a compressed 3-D CMC is complicated because the dominated damage mode is unclear. The damage may include three interactive modes: expansion mode, shear mode, and buckling mode. Although the expansion mode was concluded as the dominated damage mode for most brittle materials,[10] the 3-D fiber network may resist the expansion and play an important role in compression of the 3-D CMC. Therefore the effect of infiltration pressure on compressive strength and the related damage modes are investigated.

The lowest infiltration pressure, 0.5 MPa, for PA specimens leads to its lowest compressive strength of 24.97 MPa. Serious buckling of the fiber bundle in the compressed PA specimen is shown in Fig. 3a. At the onset of compression, the matrix crack initiates from surface ceramic layer and propagates into the fiber/matrix interface. As the crack extends, the matrix

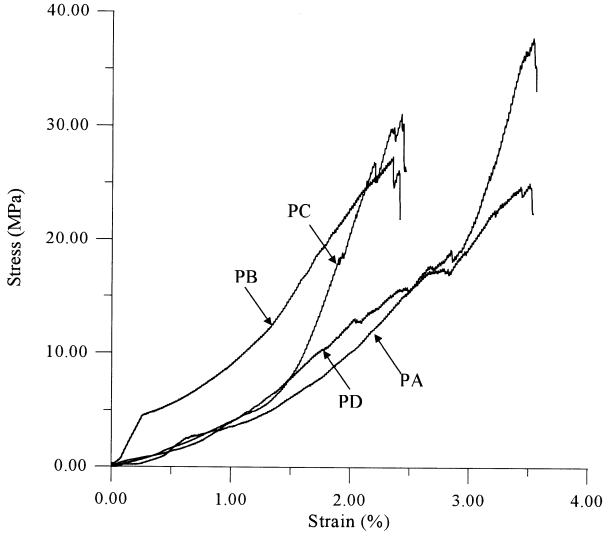

Fig. 2. Stress-strain curves for compression of PA, PB, PC, and PD specimens.

expands perpendicular to the direction of compression loading due to Poisson's effect and leads to debonding. Both debonding and compressive loading cause buckling of the fiber bundle. As shown in Fig. 2, the gradual slope in the curve for PA specimen indicates its lowest modulus of 1.392 GPa among four compressed specimens. Low infiltration pressure prevents infiltration of alumina particles into fiber bundles. As a result, low green density (Table 1) as well as higher porosity is obtained, resulting in lower modulus and weak interface. Therefore, under compression the crack propagates through weak interface and causes debonding. Besides, transverse fiber bundles become compliant due to poor infiltration. Without strong confinement force from transverse fiber bundles, serious buckling of the longitudinal fiber bundle occurs.

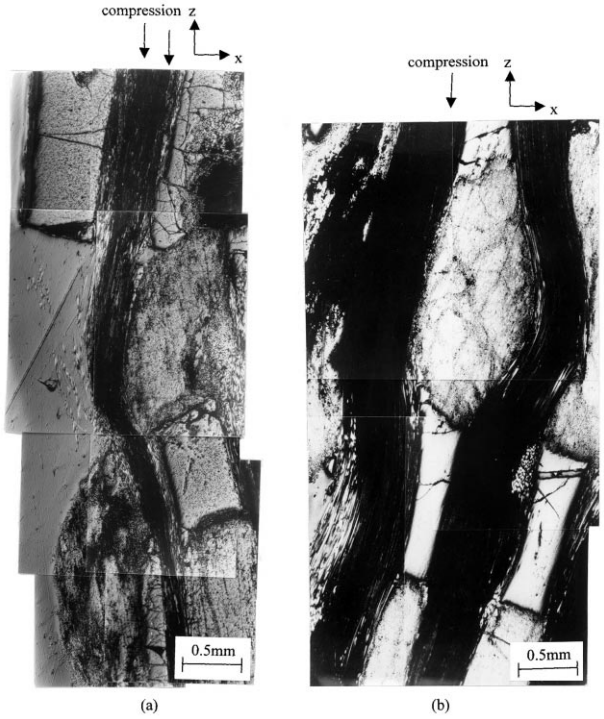

Fig. 3. (a) Serious buckling of the fiber bundle in the PA specimen in compression, (b) intermediate buckling of the fiber bundle in the PB specimen in compression.

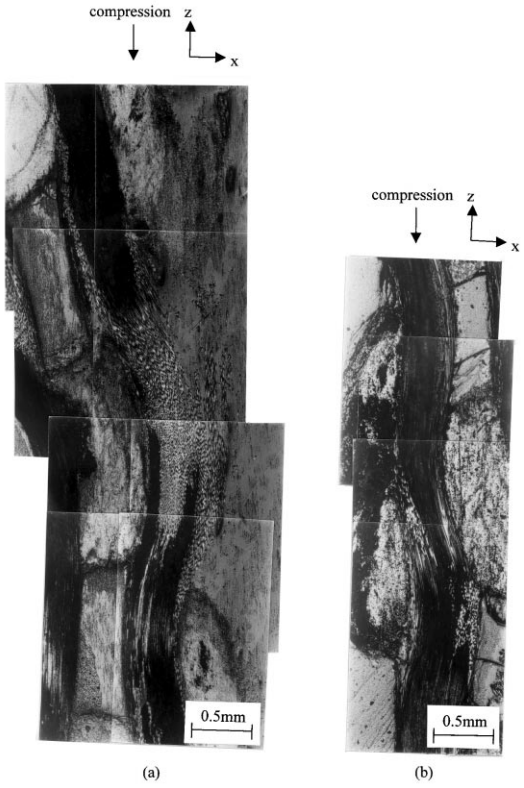

Fig. 4. (a) Moderate buckling of the fiber bundle in the PC specimen in compression, (b) slight buckling of the fiber bundle in the PD specimen in compression.

The infiltration pressure for PB specimens is 0.75 MPa, which is higher than that of PA specimens and results in higher compressive strength of 27.32 MPa and higher modulus of 1.496 GPa. Higher infiltration pressure results in better infiltration of sol/particle mixture, leading to better packing density of the particles. This enhances interfacial strength and increases compressive strength. As shown in Fig. 3b, intermediate buckling of two fiber bundles in the specimen is observed, which is less serious than that in the PA specimen. The buckling also causes cracks in inter-bundle regions among longitudinal and transverse fiber bundles, and deformation of transverse fiber bundles originally in a rectangular shape.

Similarly, the higher infiltration pressure of 1.0 MPa for PC specimens than for PB specimens leads to higher compressive strength of 31.07 MPa and modulus of 3.042 GPa. As shown in Fig. 4a, compression causes moderate buckling of the fiber bundle and leads to fiber breakage at the convex side. Few cracks occur in the transverse fiber bundle due to buckling of longitudinal bundle.

For PD specimens, the infiltration pressure is 1.25 MPa, which is the highest among four compressed specimens and results in the highest compressive strength of 37.69 MPa and modulus of 4.065 GPa. This result is due to better matrix strength caused by higher composite green density. As shown in Fig. 2, the slope for PD promptly increases when the strain is larger than 2.8%. The curve implies the microstructure evolution in the compressed 3-D ceramic composite. At the beginning of compression, shear force causes matrix microcracks inside the fiber bundle. Later, compression loading tends to close the microcracks and leads to gradual increase of modulus of the composite indicated by the slope of stress-strain curve before strain of 2.8%. As the strain is larger than 2.8%, the matrix begins to expand due to Poisson's effect, but at the same time is constrained by the transverse fiber bundles, leading to rapid increase of the slope (modulus). Finally, transverse fiber bundles can not provide sufficient confinement force, and therefore compression causes failure of the composite by the buckling mode. As shown in Fig. 4b, the longitudinal fiber bundle only slightly buckles because better confinement force is provided through stronger interface, denser matrix, and 3-D fiber network.

3.2. Flexural strength and damage

As shown in Fig. 5, flexural strength of BA, BB, BC, and BD specimens decreases with silica sol viscosity according to an exponential decay function. Flexural stress strain curves for BA, BB, BC, and BD specimens are depicted in Fig. 6. Four curves indicate similar trend except for load history after maximum load, affected by sol viscosity. A typical flexural damage configuration is

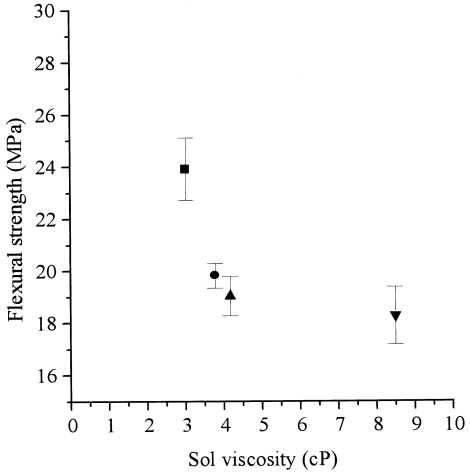

Fig. 5. Flexural strength as a function of sol viscosity for 3-D ceramic matrix composites.

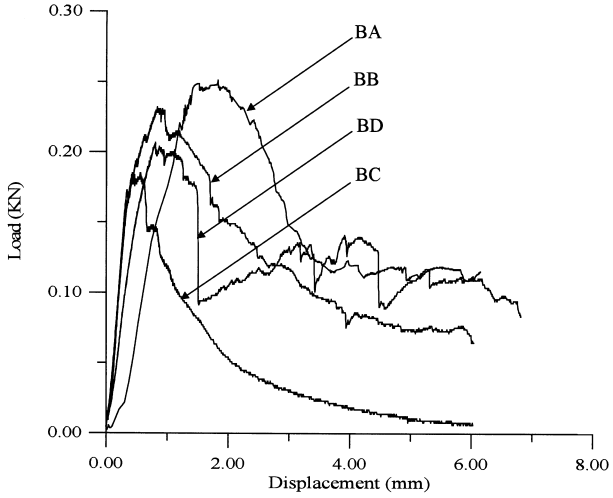

Fig. 6. Flexural load-displacement curves for BA, BB, BC, and BD specimens.

shown in Fig. 7. At the onset of flexural test, linear elastic behavior on initial stage of the stress–strain curve indicates that the ceramic matrix undertakes most of the loading. As the loading increases, matrix cracks occur and propagate to the interface. The nature of interface was affected by sol viscosity. At maximum load, a lot of fibers break followed by fiber pull-out, resulting in the reduction of flexural loading. Due to the constraint of 3-D fiber network, the crack can only detour around fibers; therefore, stress–strain curve gradually descends and the composite fails in a dissipative manner. The effect of sol viscosity on flexural strength and damage mode of the four specimens is then discussed.

For BA specimens the viscosity of silica sol is 3.02 cP, which is the lowest among four bended specimens, leading to the highest flexural strength of 23.92 MPa. The lowest viscosity of silica sol results in the good

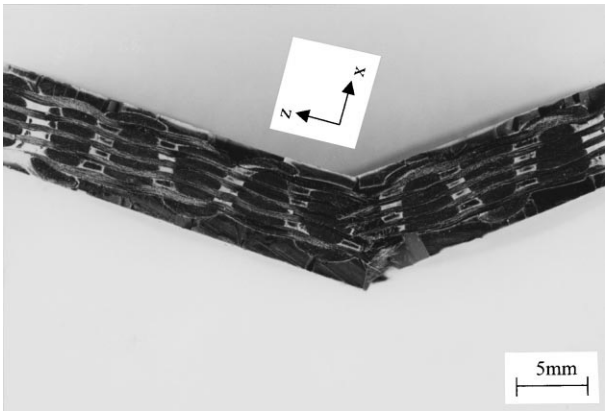

Fig. 7. Macroscopic failure of specimen under three-point bending.

infiltration for BA specimens, and yield highest composite green density as shown in Table 1. This should insure better wetting and contact at the interface and therefore leads to better interfacial strength. Under bending, the crack is difficult to propagate through better interface; instead it tends to break strong carbon fibers and yields higher flexural strength. As shown in Fig. 8a, better interface leads to bundle pull-out, adhesion of matrix on the fibers, and fiber fracture. Those damage modes correspond to the highest flexural strength of the BA specimen among four bended specimens.

The higher viscosity of silica sol for BB than for BA specimens leads to lower flexural strength of 19.8 MPa. The higher viscosity prevents the infiltration of the matrix materials and results in weaker interface as well as lower flexural strength. As shown in Fig. 8b, fiber pull-out is found in the BB specimen, contributing to lower flexural strength. Similarly, higher viscosity of silica sol for BC specimens than for BB specimens leads to lower flexural strength of 19.03 MPa. SEM observation of failure of the BC specimen in Fig. 9a shows extensive debonding and pull-out of fibers in y and z directions.

The highest viscosity of silica sol 8.50 cP for BD specimens among four bended specimens results in the lowest strength of 18.27 MPa. It is found in the load–displacement curve (Fig. 6) that the curve rebounds after it drops sharply from the maximum load. This trend is different from other curves probably due to more contribution of 3-D fiber network. The sharp drop of the curve from the maximum load infers extensive debonding in three directions (x, y, and z) because the highest sol viscosity would result in the weakest interface. Thereafter, the curve ascends because the crack deflects around 3-D fiber network. Extensive fiber pull-out (Fig. 9b) contributes to the local rise of the curve until the composite fails.

Low flexural strengths of four bended specimens suggest that the fiber degrade at the processing temperature

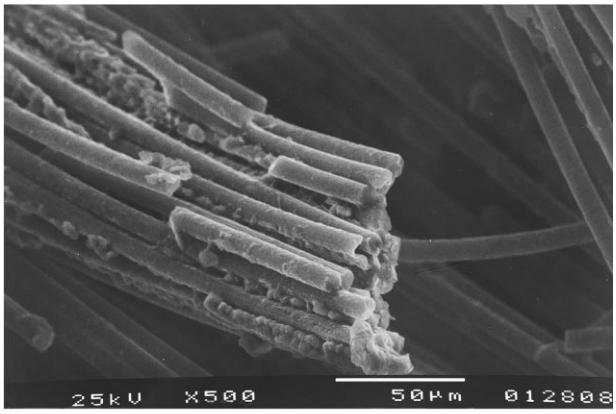

(a)

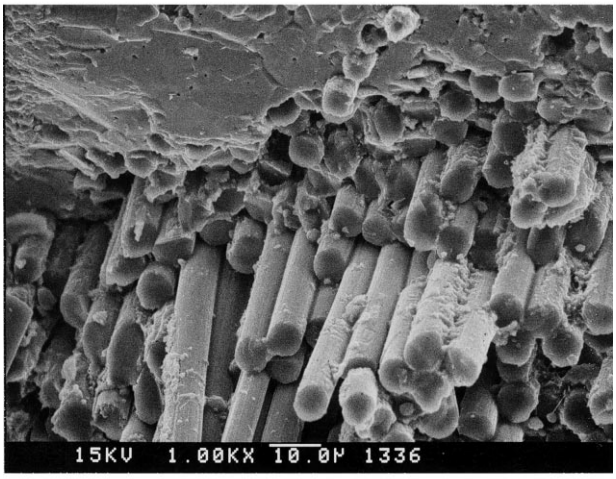

(b)

Fig. 8. (a) Failure mode of the BA specimen under bending showing bundle pull-out, (b) failure mode of the BB specimen in bending showing extensive fiber pull-out.

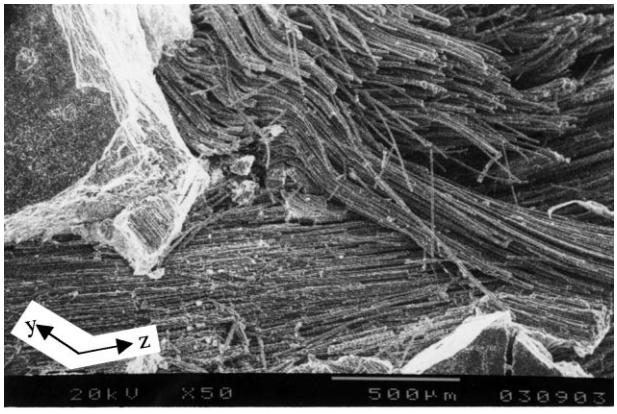

(a)

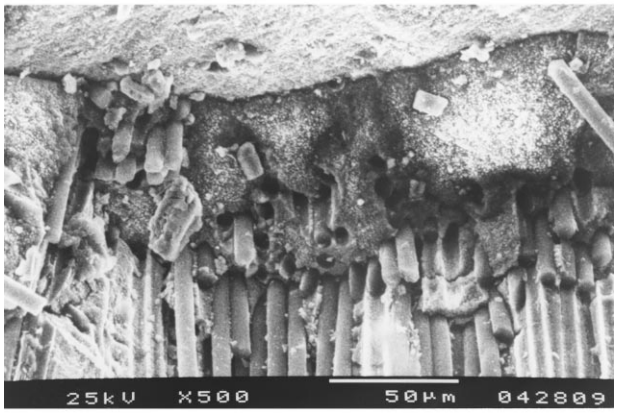

(b)

Fig. 9. (a) Failure mode of the BC specimen under bending showing fiber pull-out, breakage, and undulation, (b) failure mode of the BD specimen under bending showing extensive fiber pull-out.

and less fibers oriented in the loading direction, compared to unidirectional composites.[11]

3.3. Impact behavior

The impact energy of four impacted specimens IA, IB, IC, and ID as a function of silica sol viscosity is shown in Fig. 10. It is found that the impact energy increases linearly with sol viscosity. The correlation between impact energy and impact damage modes is discussed as follows.

The lowest viscosity of silica sol for IA specimens results in the lowest impact energy of 8.81 kJ/m^2. The low viscosity of silica sol enhances the infiltration of the mixture of silica sol and alumina particles according to Darcy's law.[13] A typical impact damage configuration of IA specimens is shown in Fig. 11a. At onset of impact, the impact loading simultaneously causes fiber breakage and matrix cracking at the impact site. The impact causes the crack to propagate across the interface and penetrate the composite instead of detouring through interface. White surface matrix layer still attaches well with the fiber preform, suggesting good interfacial bonding. Eventually the specimen broke into two pieces. Figure 11b shows smooth broken surface parallel to the impact loading direction in the IA specimens. This leads to lower impact energy for the lack of local damage mode for energy absorption.

For IB specimens, the medium-low viscosity of silica sol leads to impact energy of 9.46 kJ/m^2. As shown in Fig. 12a, the specimen also broke into two pieces, and white surface matrix layer detaches seriously from the fiber preform on left-hand side. Further, separation of fiber bundles suggests that interfacial bonding be weaker than that of IA specimens. SEM observation on IB specimen (Fig. 12b) shows a rough crack surface indicating a damage mode of crack deflection. This local damage mode contributes to higher impact energy of IB than that of IA.

For IC specimens, the medium-high viscosity of silica sol leads to higher impact energy of 9.5 kJ/m^2. The damage configuration and failure modes are shown in

Figs. 13a and b, respectively. The specimen broke into two pieces, and weak interfacial bonding was observed as indicated by separation of fibers in Fig. 13a. Failure modes of IC specimens show more debonding for higher energy absorption.

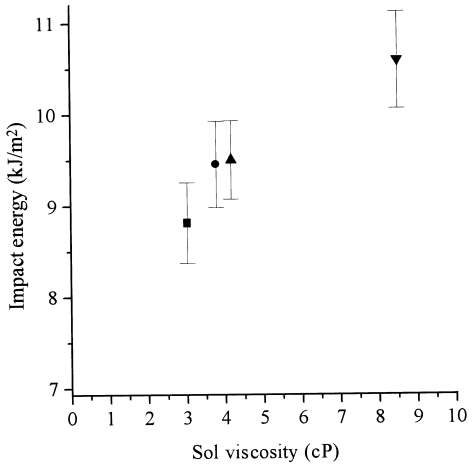

Fig. 10. Impact energy as a function of silica sol viscosity for 3-D ceramic matrix composites.

The highest viscosity of silica sol for ID specimens results in the highest impact energy of 10.5 kJ/m^2. This value is approximately the same as critical rate of release of strain energy (10.3 kJ/m^2), G_{IDm}, for 3-D Al_2O_3/SiO_2 from Ref. 9. The highest viscosity prevents good infiltration and results in lowest packing density of alumina particles in the 3-D preform, indicated by the lowest green density shown in Table 1. This leads to weak interface. As shown in Fig. 14a, the specimen does not completely separate. Upon impact, the loading causes crack to partially penetrate the composite. As the impactor proceeds, matrix cracks propagate through weak interface and this dissipates most of the impact energy before complete breakage of the composite. Therefore, there are some unbroken fibers remained to connect two broken pieces of specimen. Fig. 14b shows extensive fiber pull-out indicated by holes in the matrix, and crack deflection indicated by rather rough fracture surface. More damage modes contribute to better energy absorption.

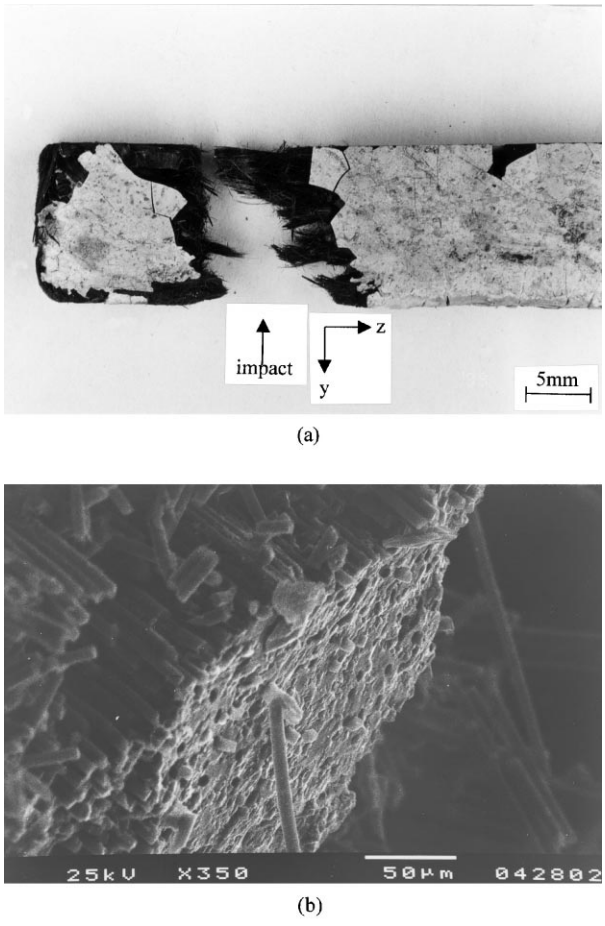

Fig. 11. Impact damage for the IA specimen showing (a) complete breakage of the composite and adhesion of surface layer, and (b) smooth fracture surface.

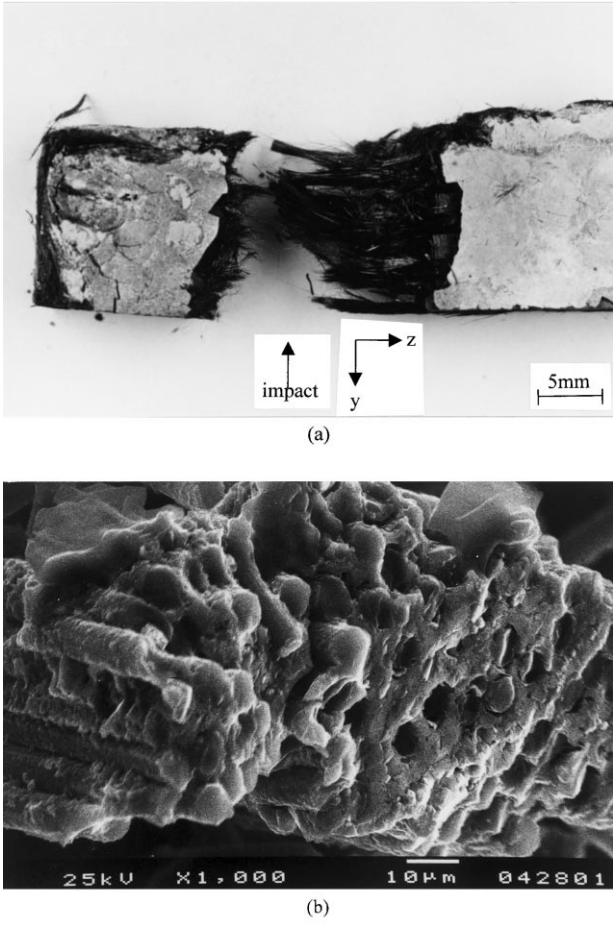

Fig. 12. Impact damage for the IB specimen from (a) complete breakage of the composite and separation of surface layer, and (b) remained holes after fiber pull-out.

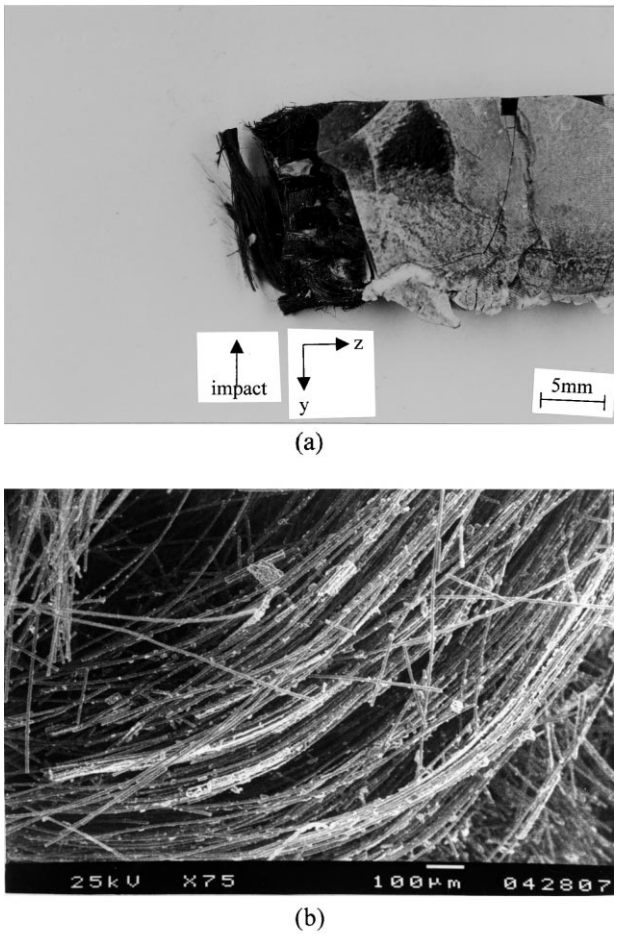

Fig. 13. Impact damage for the IC specimen from (a) complete breakage of the composite, and (b) extensive fiber bending and pull-out.

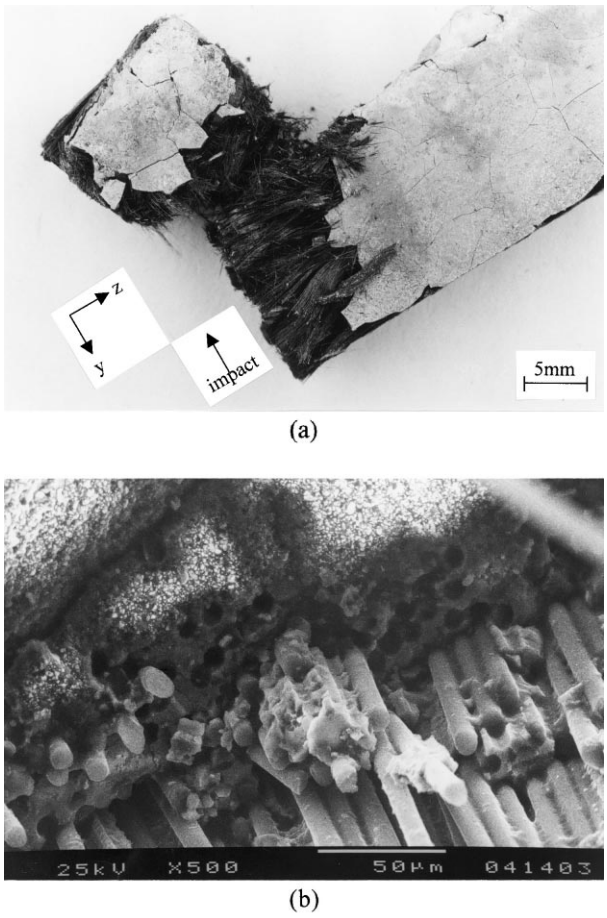

Fig. 14. Impact damage for the ID specimen from (a) bridging of the broken composite by unbroken fibers, and (b) extensive fiber pull-out.

3.4. Volume fraction of silica

The impact damage modes are also influenced by the matrix composition which is relative to volume fraction of silica. To predict the volume fraction of silica in silica/alumina matrix for the 3-D green composite, the packing density of alumina particles must be assumed. The packing density can be either 52.3% via simple cubic packing or 60% via hexagonal packing, depending on sol viscosity. For the sol with lower viscosity, the alumina particles can flow easily and packing individually during infiltration process; therefore, the particles tend to pack densely as a hexagonal packing. The empirical data for the volume fraction of silica are shown in Table 2. For the sol with viscosity of 3.02 and 3.78 cP, volume fraction of silica would be 0.65 and 2.1%, respectively. In contrast, alumina particles in the higher viscosity sol would lead to simple cubic packing, resulting in volume fraction of silica as 2.68% (4.17 cP) and 2.8% (8.50 cP).

Based on prediction of volume fraction of silica, the reaction between silica and alumina can be involved to modify the matrix composition. A schematic diagram shown in Fig. 15 can be used to summarize the influence of silica sol viscosity on matrix composition of 3-D ceramic matrix composites. Fabricated by the lowest sol viscosity, more alumina particles can be infiltrated into intra-bundle pores among fibers of IA specimens under lower viscous force. When the sol viscosity increases, the particles become more and more difficult to infiltrate the pore, as can be seen in the change of green density in Table 1 from IB to ID. After hot-pressing, silica sol can react with alumina particles and produce mullite matrix, depending on stoichiometric proportion of alumina to silica.[14] Therefore, it is possible to simultaneously detect silica, alumina, and mullite in the matrix in which their fracture toughness ranks from high to low.[15] For IA specimens, a very small amount of silica (Table 1) may react with alumina to produce mullite as a thin surface layer around alumina grains. Thus, the composition of IA would be a large amount of alumina plus little mullite. For IB specimens, more silica and less alumina tend to yield some mullite, however, the residual silica can toughen the matrix and overwhelm the reduction of

Table 2
Predicted volume fraction of silica in silica/alumina matrix for the 3-D green composite

Sol viscosity (cP)	Volume of silica sol (cm^3)	Weight of dried gel (g)	Weight of silica (g)	Volume of silica (cm^3)	Packing density of alumina (%)		Volume fraction of silica (%)	
					Cubic	Hexagonal	Cubic	Hexagonal
3.02	175	4.2	3.78	1.72	52.3	0.6	0.88	0.65
3.78	175	13.6	12.36	5.62	52.3	0.6	2.8	2.1
4.17	175	13.44	11.62	5.28	52.3	0.6	2.68	1.97
8.50	175	13.54	12.12	5.51	52.3	0.6	2.8	2.06

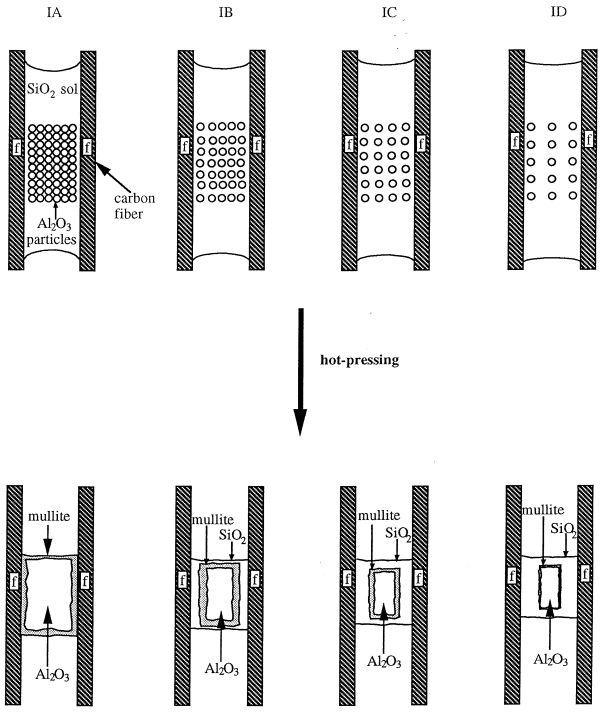

Fig. 15. The schematic diagram for mechanisms that influences impact response of IA, IB, IC, and ID specimens.

toughness caused by mullite. Eventually, IB has higher impact energy than IA. For IC specimens, the composition is similar to that of IB except for more residual silica, and this leads to slightly higher impact energy. Although there is a great amount of silica in ID specimens, only few amount of mullite can be produced due to a small amount of alumina particles. Therefore, a large amount of residual silica leads to the highest impact energy of ID specimens.

4. Conclusions

The effect of processing parameters on impact behavior, compressive strength, and flexural strength of 3-D ceramic matrix composites has been examined. The silica sol viscosity affects impact performance of composites, not only because it influences the flow of sol/particle mixture, but also the matrix composition. The ease of the flow of the mixture under lower viscosity led to denser particle packing both in inter-yarn and intra-yarn pores, and this resulted in better interfacial bonding after hot-pressing, and lower impact energy. Further, less residual silica and some mullite fabricated by lower sol viscosity caused lower impact energy of composites due to more brittle nature of mullite than silica. With sol viscosity from low to high, the corresponding failure modes of specimens IA, IB, IC, and ID are straight cracks, deflected cracks, debonding, and debonding and pull-out. With more failure modes and energy dissipative mode such as pull-out, ID specimens possess highest impact energy.

It was found that the compressive strength of the composites increased with infiltration pressure according to a parabolic function. Higher infiltration pressure assisted the infiltration of the mixture of sol and particles into intra-bundle pores, leading to dense matrix with less porosity. It was found that fiber buckling is unavoidable for undulated fibers in compressed 3-D composites. The dense matrix is expected to provide stronger interface and lateral confined force. This reduces buckling of fibers and contributes to better compressive strength. The flexural strength of the composites was found to decrease with sol viscosity according to an exponential decay function. The low sol viscosity leads to dense matrix and strong interface, and these result in high flexural strength because high flexural strength is usually accompanied by strong interface. Furthermore, for specimens under the same infiltration pressure and sol viscosity the flexural strength was lower than the compressive strength. This is due to the nature of brittle materials that compression loading inhibits the crack propagation, while tensile loading associated with the flexural test promotes crack propagation.

It was further found that the improved toughness of the 3-D composites was achieved at the expense of the strength. Although higher compressive and flexural strengths were not obtained in this paper, a contribution was made on the influence of processing parameters on both strengths and impact performance. Further, the findings of correlation between the two strengths and impact response should provide valuable information for the community of ceramic matrix composites.

Acknowledgements

The authors are grateful to National Science Council, Taiwan ROC for financial support under contract: NSC 88-2216-E-035-009, and Professor Wen-Shyong Kuo in Department of Aeronautical Engineering, Feng-Chia University, Taiwan for providing 3-D preform.

References

1. Liu, H. K. and Parvizi-Majidi, A., Effect of particle additions on drying stresses and green density of sol–gel processed three dimensional ceramic matrix composites. *J. Am. Ceram. Soc.*, 1998, **81**, 1824–1828.
2. Liu, H. K., Kuo, W. S. and Lin, B. H., Pressure infiltration of sol/gel processed short fiber ceramic matrix composites. *J. Mater. Sci.*, 1998, **33**, 2095–2101.
3. Liu, H. K., Investigation on the pressure infiltration of sol–gel processed textile ceramic matrix composites. *J. Mater. Sci.*, 1996, **31**, 5093–5099.
4. Velamakanni, B. V. and Lange, F. F., Effect of interparticle potentials and sedimentation on particle packing density of bimodal particle distributions during pressure filtration. *J. Am. Ceram. Soc.*, 1991, **74**(1), 166–172.
5. Chou, T. W. and Ko, F. K., *Textile Structural Composites*. Elsevier Science Publishers B. V., The Netherlands (Chapter 3).
6. Kuo, W. S. and Lee, L. C., Impact response of 3-D woven composites reinforced by consolidated rods. *Polymer Composites*, 1998, **19**, 156–165.
7. Sugiyama, F., Ishikawa, T., Ogawa, K. and Nishida, T., Fracture strength of fiber-bonded ceramic composite subjected to static and impact bending. *JSME Int. J. A. Solid Mech. and Mat. Engrg.*, 1998, **41**, 495–502.
8. Phillips, D. C., Park, N. and Lee, R. J., The impact behavior of high-performance ceramic matrix composites. *Comp. Sci. Tech.*, 1990, **37**, 249–265.
9. Macke, T., Quenisset, J. M., Neuilly, D., Rocher, J. P. and Naslain, R., A comparative study of the impact behavior of ceramic matrix composites. *Comp. Sci. Tech.*, 1990, **37**, 267–278.
10. Lankford, J., The effect of hydrostatic pressure and loading rate on compressive failure of fiber-reinforced ceramic-matrix composites. *Comp. Sci. Tech.*, 1994, **51**, 537–543.
11. Nakano, K., Kamiya, A., Nishino, Y., Imura, T. and Chou, T. W., Fabrication and characterization of three-dimensional carbon fiber reinforced silicon carbide and silicon nitride composites. *J. Am. Ceram. Soc.*, 1991, **78**, 2811–2814.
12. Wang, Z. G., Hashin, C. L. Z., Rosen, B. W. and Yen, C. W., Mechanical behavior of a cross-weave ceramic matrix composite. *J. Mater. Sci.*, 1991, **26**, 4571–4578.
13. Dullien, F. A. L., *Porous Media: Fluid Transport and Pore Structure*. Academic Press, New York (Chapter 4).
14. Liu, H.-K. and Lin, B.-H., The effect of sol/particle reaction on properties of two-dimensional ceramic matrix composites. *Materials Letters*, 2000, submitted.
15. Warren, R., *Ceramic Matrix Composites*. Chapman and Hall, New York (Chapter 2).